



ARTICLE

A Novel Magnetic Carbon Based Catalyst Synthesized from Reed Straw and Electric Furnace Dust for Biodiesel Production

Fuping Wang¹, Lele Kang¹, Rui Ji¹, Tianji Liu¹, Qing Yu¹, Di Gao¹, Xiaoman Wang¹, Yitong Wang^{1,*} and Jie Yang^{2,*}

¹College of Metallurgy and Energy, North China University of Science and Technology, Tangshan, 063210, China

²Qian'an College, North China University of Science and Technology, Qian'an, 064400, China

*Corresponding Authors: Yitong Wang. Email: wangyt@ncst.edu.cn; Jie Yang. Email: wangcong@ncst.edu.cn

Received: 28 August 2021 Accepted: 21 October 2021

ABSTRACT

In the era of serious greenhouse gas emission and energy shortage, it is necessary to use solid waste to prepare new renewable materials. In this work, the potential application of reed straw and electric furnace dust was explored. Firstly, magnetic carbon carrier (EFD&C) was prepared by high temperature calcination, and then magnetic carbon catalyst (SM@EFD&C) was prepared by activation of sodium methoxide. The catalyst was used to prepare biodiesel by transesterification reaction to test its activity and stability. Reed biochar, EFD&C and SM@EFD&C were detected by Diffraction of X-rays (XRD), Fourier transform infrared (FT-IR), Inductively coupled plasma (ICP), Scanning electron microscope (SEM), Transmission electron microscope (TEM), Brunauer-Emmett-Teller (BET), Vibrating sample magnetometer (VSM), Temperature programmed desorption of CO₂ (CO₂-TPD) and Thermogravimetric analysis (TG-DTG). The results showed that SM@EFD&C catalyst had some characteristics including porous structure, easy adsorption and better magnetism. Under the reaction conditions of 65°C for 2 h with 6 wt% catalyst and methanol/oil molar ratio of 15:1, the biodiesel yields from reed biochar and EFD&C were only 4.88 wt% and 0.03 wt%, respectively, while the yield from SM@EFD&C catalyst reached 93.14 wt% (89.84 wt% after 7 cycles) under the same conditions, which proved that it had good catalytic activity and stability when used in biodiesel production. This study is of great significance of carbon dioxide emission reduction and environmental protection.

KEYWORDS

Reed biochar; electric furnace dust; magnetic biochar catalyst; biodiesel; environmental protection

1 Introduction

In 2015, representatives from 195 countries reached the Paris Climate Agreement (greenhouse gas emission in countries around the world need to reach a new level) [1]. Carbon dioxide produced by the burning of fossil fuels accounts for 76% of the total global greenhouse gas [2]. Therefore, developing environmentally friendly renewable energy is of the great significance to environmental protection. Biomass energy ranks fourth in the world's total energy consumption after coal, oil and natural gas. Within the next century, it is estimated that biomass fulfills half of the world's energy demand [3]. Therefore, the use of existing waste biomass resources to produce high value-added products plays a positive role in achieving carbon peak and carbon neutrality. Biomass energy refers to heat energy



produced by non-fossil biological materials [4], including biomass derived biofuels, agricultural and forestry crops and their wastes, aquatic plants, animal dung and urban and industrial organic wastes [5]. Due to its characteristics including large surface area, rich porous structure, high stability, a wide range of raw materials and low preparation cost [6,7], biochar has been widely applied in many fields, such as soil improvement [8], agricultural production [9], sewage treatment [10] and waste management [11], and have attracted many attentions in the preparation of biochar from biomass. Biochar can be prepared by pyrolysis, hydrothermal carbonization, template method and activation method of biomass under conditions of little or no oxygen [12]. During the process of biomass conversion to biochar, organic carbon can be transformed into inorganic carbon, thus achieving carbon fixation to reduce net carbon emissions [13]. Due to the characteristics of biochar itself, it shows good performance when used as a catalyst carrier, and does not have a negative impact on the catalytic process and product. Compared with other carriers, biochar has excellent stability in alkaline or acidic media. Meanwhile, biochar has a high specific surface area, which can better distribute metal active substances on it, thus improving the stability and effectiveness of the catalyst [14]. Qiu et al. [15] used biochar as a catalyst for the upgrading of bio-oil from rice husk pyrolysis. The results showed that biochar can promote the production of hydrocarbon, reduce the oxygen content in bio-oil, and improve bio-oil quality. Foroutana et al. [16] prepared a new heterogeneous catalyst (algae biochar/CaO/K₂CO₃), and used it to produce biodiesel by transesterification reaction to waste edible oil and methanol with 98.83% biodiesel yield obtained.

Reed is a kind of gramineous plant, mainly distributed among shallow water areas and wetlands, and has properties including easy reproduction and high annual yield, so it is an important ecological revetment plant. However, reed straw has almost zero application values due to its wide distribution and low energy density [17]. The annual output of reed straw in China exceeds 2 million tons, accounting for about 6% of the global total output. A large amount of reed straw is not utilized as a resource every year [18]. Reed straw has high carbon content and low inorganic content, which can be used as a low-cost resource for the preparation of biochar [19]. Electric furnace dust (EFD) is a by-product from electric arc furnace steelmaking process. Every ton of steel produced will produce 10–20 kg EFD powder [20], which is a huge solid waste in the metallurgical industry. EFD powder contains a certain amount of iron or iron compounds with considerable magnetism [21], so it can be used as raw materials for preparing magnetic catalysts. Kamali et al. [22] used EFD powder as a raw material to prepare magnetic MgFe₂O₄-CaFe₂O₄ photocatalyst, which was used in the degradation of methylene blue with good activity and stability. In recent years, some studies of magnetic catalysts have attracted much attention due to being easily separated from reactants [23]. So comprehensive utilization of EFD powder and reed straw has certain practical significance in climate and ecological protection. Biodiesel is fatty acid methyl esters produced from transesterification or the esterification reaction of vegetable oil or animal fat and methanol [24]. In addition to similar properties to fossil diesel, it also has advantages, such as renewability and low carbon dioxide content [25]. Among methods of biodiesel production, transesterification is the preferred method of producing high-quality biodiesel [26]. Adding acidic or basic catalysts in the transesterification reaction can greatly improve biodiesel yield and quality. Rich sources of raw materials for catalyst preparation, simple catalyst preparation methods, and low-cost catalyst preparation method have always been the bottleneck in the industrial application of biodiesel. Therefore, we used reed stalks and electric furnace dust as raw materials for biodiesel production, which not only enabled the effective use of solid waste, but also solved the problems of energy depletion and environmental pollution.

In this study, reed straw was used as raw material for biochar preparation, and the EFD powder was used as a magnetic core for magnetic biochar preparation. Synthesized magnetic biochar was impregnated with sodium methoxide and calcined to produce carbon-based catalyst (SM@EFD&C), and its activity and stability were tested with transesterification of soybean oil. Catalytic materials are characterized to understand the activation mechanism.

2 Materials and Methods

2.1 Materials

Sodium methylate ($\geq 97\%$), methanol (99.5%), methyls of heptadecanoate ($\geq 99\%$), palmitate ($\geq 99.0\%$), linoleate (99.5%), oleate ($\geq 99.0\%$), linoleate ($\geq 99\%$), stearate ($\geq 99.5\%$) and palmitoleate were purchased from Aladdin Industrial (Shanghai). Ethanol absolute was bought from Yongda Chemical Reagent Company Limited (Tianjin). Hydrochloric acid (37.5%) and dichloromethane ($\geq 99.5\%$) were purchased from Tianjin Kaixin Chemical Industry and Jingdong Tianzheng Precision Chemical Reagent Factory in Tianjin, respectively. Soybean oil (acid value (AV) of 0.06 mg KOH/g and molecular weight (MW) of 709.74 g/mol) was from a supermarket (Tangshan). The reed straw was from the wetland in the Caofeidian district (Tangshan). Raw EFD powder (dried at 105°C for 4–5 h, $\leq 75 \mu\text{m}$) with elements of Fe (54.84 wt%), Zn (1.42 wt%), Mn (1.08 wt%), Mg (0.55 wt%), Ca (1.65 wt%), Al (0.25 wt%) and Na (0.25 wt%) was from a steel factory in Tangshan.

2.2 Catalyst Preparation

Reed straw (20 g) was washed with deionized water, and dried at 105°C overnight in an oven (DGG-9140B, Shanghai Senxin Experimental Instrument Co., Ltd., Shanghai). The dried sample was ground in a crusher with a size of $\leq 3 \text{ mm}$. Raw EFD powder (10 g) and concentrated hydrochloric acid (50 mL) were added in a beaker with mechanical stirring to pretreatment, and named as pretreated EFD suspension. Reed straw powder (20 g), all pretreated EFD suspension and deionized water (450 mL) were placed in a beaker with mechanical stirring for 20 min, stand for 12 h, washed to pH 6–7, filtered and dried at 105°C overnight. Raw reed straw and obtained sample were calcined at 600°C in 2 h [27] in a tubular furnace (SK-ES08143, Zhongyi Guoke Technology Co., Ltd., Beijing) with N_2 flow rate of 200 mL/min and heating rate of 5 °C/min, ground with a size of $\leq 75 \mu\text{m}$, and named as reed biochar and EFD&C, respectively. EFD&C powder and CH_3ONa were mixed with mass ratio of 1/1, then mixture and deionized water (20 mL) were added into a 50 mL sealed serum bottle and heated at 75°C in 2 h with magnetic stirring in an oil bath (DF-101S, Shanghai Lichen Bangxi Instrument Technology Co., Ltd., Shanghai), and dried at 105°C on a heating plate (ECH-20D microcomputer temperature control heating plate, Shanghai Xinyi Microwave Chemistry Technology Co., Ltd., Shanghai) overnight. The dried sample was heated at 600°C with a heat rate of 5°C/min in a tubular furnace under a nitrogen atmosphere (N_2 flow rate of 200 mL/min) for 2 h, the calcined powder was ground with a size of $\leq 75 \mu\text{m}$, and named as SM@EFD&C.

2.3 Catalyst Characterization

Crystal characteristics of reed biochar, EFD&C and SM@EFD&C catalysts were detected with X-Ray Diffraction (XRD, D8 Advance, Bruker AXS GMBH, Karlsruhe, Germany) with $\text{CuK}\alpha$ radiation (40 kV and 200 mA). The morphology and element concentrations on the surface of catalysts were examined with scanning electron microscope-X-ray energy dispersive analysis (SEM-EDX; SU8020, Hitachi, Tokyo) and transmission electron microscope (TEM; Tecnai G2 F30 S-TWIN, FEI, Hillsboro, OR). Their BET (Bruner-Emmett-Teller) surface area, pore volume and pore diameter were analyzed using automatic physical adsorption instrument with N_2 adsorption (ASAP 2460, Micromeritics Instrument Co., Ltd., Northcross, GA). Their basicity was measured from 100°C to 600°C with CO_2 -temperature programmed desorption (CO_2 -TPD, AutoChem II 2920, Micromeritics Instrument Co., Ltd., Norcross, GA). Functional groups on the surface of samples were measured with Fourier transform-infrared spectra (FT-IR, Nexus, Thermo Fisher Scientific Co., Ltd., Waltham, MA) from 400 to 4000 cm^{-1} using the standard KBr disc method. Saturation magnetization was detected by vibrating sample magnetometer (VSM, SQUID-VSM, MPMS3, Quantum Design International, San Diego, CA). Elements in synthesized samples and raw EFD powder were analyzed by inductively coupled plasma-optical emission spectrometer (ICP-OES,

Prodigy 7, Leeman Labs Inc., USA) and an element analyzer (Vario EL III CHONS, Elementar Analysensysteme GmbH, Hanau, Germany). The thermogravimetric analysis (TG/DTG) was performed in a model LDX-HCT-3 (Beijing Henven Scientific Instrument Factory, Beijing), with the temperature ranging between 30 and 1000°C and a heating rate of 10 °C min⁻¹, under a nitrogen atmosphere with a flow of 50 mL min⁻¹.

2.4 Synthesis and Analysis of Biodiesel

2.4.1 Synthesis of Biodiesel

Soybean oil (0.01 mol) and methanol (methanol/oil molar ratio of 15/1), catalyst (6 wt%, relative to the mass of soybean oil) were added into a sealed glass bottle with a rubber aluminum cap under an oil bath (DF-101S, Shanghai Lichen Bangxi Instrument Technology Co., Ltd., Shanghai) at 65°C for 2 h with magnetic stirring. After the reaction, the product in the glass bottle can be quickly divided into three parts under the influence of the external magnetic field, the top was crude biodiesel, the middle was glycerin and excess methanol, and the bottom of the glass bottle was the solid catalyst. Removed the upper biodiesel solution, filtered it with a 0.22 µm filter membrane, and dried it in a 75°C drying oven for 4 h, and then used a gas chromatograph for quantitative analysis of biodiesel.

2.4.2 Analysis of Biodiesel

After the reaction, crude biodiesel at the top was filtered with a 0.22 µm filter membrane, dried at 75°C within 4 h, then analyzed by a gas chromatograph (GC: GC-2014C, Shimadzu, Japan) with a capillary column of Rtx-Wax (30 m × Φ 0.25 mm × 0.25 µm) under analysis conditions as follows: injector temperature of 260°C, column temperature of 220°C, detector temperature of 280°C, carrier gas flow rate of 1 mL/min and a split ratio of 40:1. Heptadecanoic acid methyl ester (HAME, C17:0) was used as the internal standard for biodiesel quantitative analysis, and biodiesel yield was calculated according to standard methyl ester weights, calibration factors and peak areas. Biodiesel yield was calculated by the Formulas (1) and (2) as follows:

Weight of a FAME (i) in crude biodiesel (W_{FAMEi}) was calculated using Eq. (1):

$$W_{FAMEi} = (W_{HAME} \times A_{FAMEi}) / (A_{HAME} \times F_i) \quad (1)$$

where: W_{HAME} : Weight of HAME;

A_{FAMEi} : GC peak area for a FAME (i);

A_{HAME} : GC peak area for HAME;

F_i : Relative response factor for a FAME (i).

Biodiesel yield (wt %) was calculated using Eq. (2):

$$Biodiesel\ yield\ (wt) = \left(\sum_i W_{FAMEi} / W_{crude\ biodiesel} \right) \times 100\% \quad (2)$$

where: W_{FAME} : Weight of all FAMES in crude biodiesel;

$W_{crude\ biodiesel}$: Weight of crude biodiesel.

Calibration factors for methyls of palmitate, palmitoleate, stearate, oleate, linoleate and linolenate to HAME (determined according to the external reference method [28]) were 1.000, 0.919, 0.834, 0.936, 1.055 and 0.970, respectively.

3 Results and Discussion

3.1 XRD

The crystal characterization of reed biochar, EFD&C and SM@EFD&C catalyst was shown in Fig. 1. In Fig. 1a a typical broad diffraction peak of amorphous carbon [29], and SiO₂ crystal were found. After the reed was modified with pretreated EFD suspension, characteristic peaks at Fe₁₁Co₅, Fe₂SiO₄ and MgFe₂O₄ crystals appeared in Fig. 1b. Firstly, Fe, Mg and Co oxides reacted with concentrated hydrochloric acid to generate FeCl₃, MgCl₂ and CoCl₂, which were loaded on the surface of reed straw, then calcination at high temperature produces Fe₁₁Co₅ [30], Fe₂SiO₄ [31] and MgFe₂O₄ [32], and solid biochar was converted to gaseous CO and CO₂ to create the void in this process [33]. After impregnating with CH₃ONa solution, the diffraction peaks of Na₂CO₃ and Fe₃C crystals appeared in Fig. 1c. When impregnated in CH₃ONa (excess deionized water), CH₃ONa reacted with water to form NaOH and adhered to EFD&C. During calcination, NaOH and carbon reacted to produce Na₂CO₃ and H₂ [34], the reaction equation was as follows:



there were H₂ production and carbon loss in this process. In the preparation of activated carbon materials, alkali metal hydroxides (especially NaOH and KOH) were often used as activators to produce microporous activated carbon. The method of chemical activation presented several advantages over the physical activation, leading to materials with large specific surface area and elevated microporosity with relatively narrow pore-size distribution [35]. Therefore, the transformation process from CH₃ONa to Na₂CO₃ can also be regarded as the activation process of carbon materials, and the two have strong interactions. After the SM@EFD&C catalyst was calcined, the calcination time of the biochar will be extended, the biomass will be further decomposed into volatile organic compounds, the carbon content will be reduced [36]. In Fig. 1c, the decrease of diffraction peak of Fe₂SiO₄ and MgFe₂O₄ crystals was due to the thermal decomposition reaction of some Fe₂SiO₄ and MgFe₂O₄ with the undischarged H₂ and carbon decomposition products, Fe₃C crystals were generated by carbothermal reduction [37].

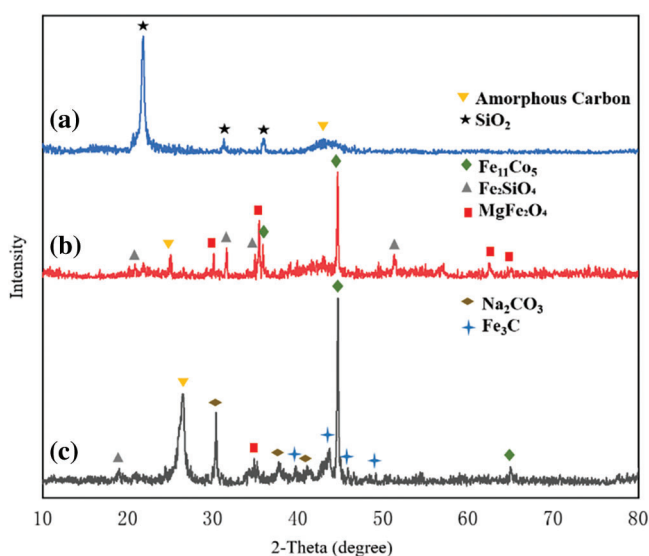


Figure 1: XRD patterns of (a) Reed biochar, (b) EFD&C and (c) SM@EFD&C

3.2 FTIR

In Figs. 2a–2c for FT-IR analysis, a characteristic band of the O-H stretching modes of the COOH at 3433 cm^{-1} [38] and C=C stretching vibration in graphite domain at 1642 cm^{-1} and 1646 cm^{-1} [39] were found. There were persistent absorption bands corresponding to the vibration of tetrahedral and octahedral complexes (M-O) at 568 cm^{-1} and 464 cm^{-1} , the acromion of these two peaks indicated the presence of other ionic states (such as Mg^{2+}) [40], it proved the formation of MgFe_2O_4 crystals (consistent with XRD results). In Fig. 2c, the occurrence of a band at 698 cm^{-1} and 880 cm^{-1} were attributed to the asymmetric stretching of CO_3^{2-} [41] and the vibration band at 1451 cm^{-1} was attributed to Fe-C [42], this was consistent with the XRD conclusion, indicated that Na_2CO_3 generated by the reaction of NaOH with carbon was connected with EFD&C support in the form of C-O-Na chemical bond. Studies have shown that due to the presence of these Na-containing groups in the carbon a supported material, which were strongly bonded and not easily leached away from the porous carbon a supported material, thus better activity and stability can be obtained [43]. The absorption band at 1014 cm^{-1} was caused by the asymmetric stretching of the Fe-Si-O peak [44] the absorption bands at 1085 cm^{-1} and 793 cm^{-1} were attributed to the general asymmetric vibration of the Si-O-Si and the stretching vibration of Si-O group [45–47].

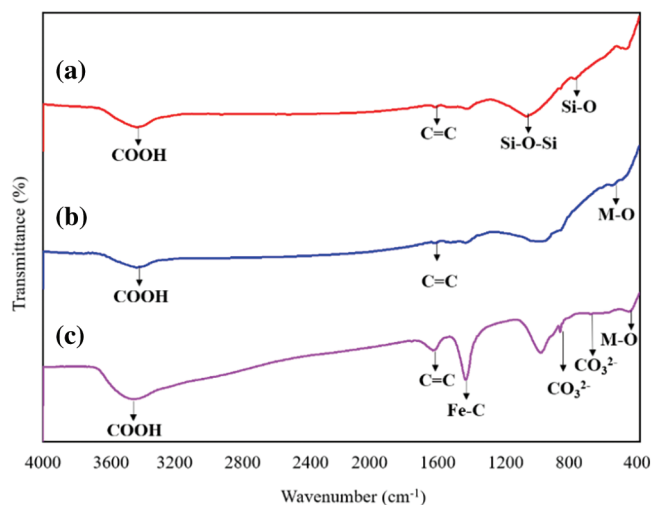


Figure 2: FT-IR spectra of (a) Reed biochar, (b) EFD&C and (c) SM@EFD&C

3.3 Element Composition and ICP

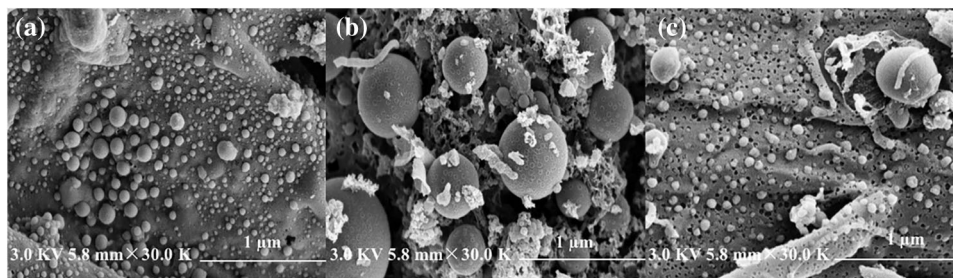
The elemental composition of reed biochar, EFD, EFD&C and SM@EFD&C catalysts were shown in Table 1. It can be seen that the elements in reed biochar were mainly C (72.23 wt%), Si (1.85 wt%) and Na (2.14 wt%), the contents of elements of Fe (0.13 wt%), Mg (0.13 wt%) and Co (0.0003 wt%) were less. After EFD was added to reed biochar, Fe content from 54.83 wt% decreased to 13.01 wt%, while other elements relative content decreased. After impregnating with CH_3ONa , content of Na from 1.54 wt% increased to 21.42 wt% and C decreased greatly. It was worth noting that we calcined biochar a second time, which was equivalent to prolong the calcination time of biochar at high temperature. The reason for the drop in biochar quantity with higher reaction time was due to further decomposition of biomass that resulted in removal of volatile organic compounds and therefore reducing the quantity of biochar [48]. A decrease of the relative content of C led to the increase of the relative content of Si element. It can be seen from Table 1, the relative decrease of C content was 28.56%, while the increase of Si and Na was 3.76% and 19.98%, respectively. Although the relative content of Na increased, the reduction in carbon was greater than the combined increase of Na and Si.

Table 1: The elemental composition of reed biochar, EFD, EFD&C and SM@EFD&C catalysts

Catalyst	C (wt%)	Si (wt%)	Na (wt%)	Fe (wt%)	Mg (wt%)	Co (wt%)
Reed biochar	72.23	1.85	2.14	0.13	0.13	0.0003
EFD	-	-	0.09	54.83	0.54	0.0025
EFD&C	64.28	0.54	1.54	13.01	0.13	0.0006
SM@EFD&C	35.72	4.30	21.42	6.78	0.13	0.0002

3.4 SEM and TEM-EDX

In Figs. 3a–3c represent SEM images of reed biochar, EFD&C and SM@EFD&C catalysts, respectively. In Fig. 3a, the surface of biochar was relatively rough with a vesicular structure of different sizes and obvious pore structures. It was caused by the carbonization of biological macromolecules (such as lignocellulose, etc.) and organic molecules during high-temperature heating [49]. The surface of EFD&C prepared after treatment with EFD suspension was porous, with spherical substances of different sizes attached to the surface. This was because the reed contained macromolecular structures (such as cellulose and hemicellulose [50]) was acid hydrolyzed, thereby reducing the carbonization of macromolecules during the pyrolysis process [51]. In Fig. 3c, the porous structure on the surface of the biochar was attached with a uniform particle structure, the distribution was relatively uniform. Combined with XRD analysis, it can be judged that these attached particles were Na_2CO_3 .

**Figure 3:** SEM images of (a) Reed biochar, (b) EFD&C and (c) SM@EFD&C

The TEM images of reed biochar, EFD&C and SM@EFD&C catalysts and corresponding EDX images were shown in Fig. 4. As can be seen from Fig. 4Aa that the surface of the reed biochar had porous morphology and vesicular structure, which was consistent with the SEM image analysis. In Fig. 4Ba, it was obvious that a large number of substances were attached of the surface of biochar, the surface had more void structures than that of reed biochar. The EDX image showed the presence of iron with a relative content of 4.78 wt%, which further indicated the formation of $\text{Fe}_{11}\text{Co}_5$, Fe_2SiO_4 and MgFe_2O_4 (Fig. 4Bb). After impregnating with CH_3ONa solution, the structure of the carbon-based surface was relatively loose, which was due to partial collapse caused by carbon thermal reaction and CO_2 induction. At the same time, because Na_2CO_3 was loaded on the surface of EFD&C, the relative content of element C on the catalyst surface was reduced. In Fig. 4Cb, the relative content of Na and O elements on the carbon-based surface were 6.02 and 6.02 wt%, which showed that Na_2CO_3 were evenly distributed on the carbon base surface, which was conducive to the catalytic reaction.

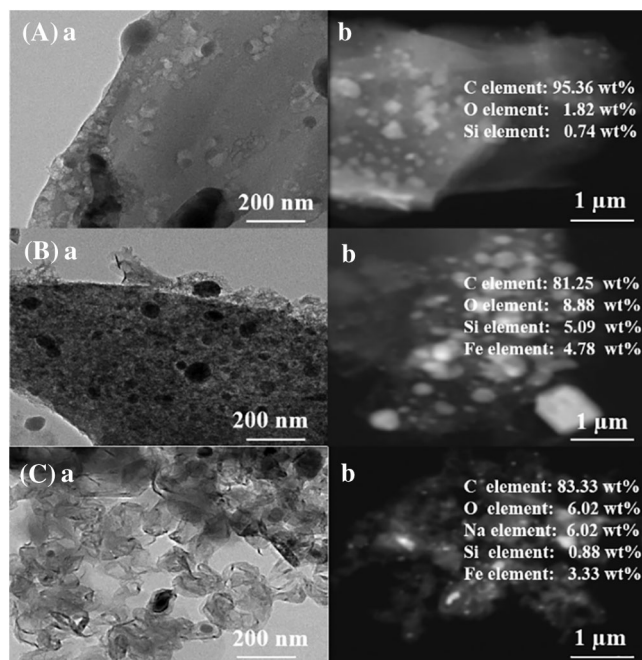


Figure 4: TEM-EDX images (a) TEM and (b) EDX of (A) reed biochar, (B) EFD&C and (C) SM@EFD&C

3.5 BET

The N_2 adsorption-desorption curves of reed biochar, EFD&C and SM@EFD&C catalysts were shown in Fig. 5. The N_2 adsorption-isotherm of reed biochar and EFD&C were a typical IV type with an adsorption hysteresis loop, which was observed in materials with a mesoporous structure. The BET specific surface area of reed biochar with $701.69 \text{ m}^2/\text{g}$, the average pore size and pore volume with 2.34 nm and $0.41 \text{ cm}^3/\text{g}$, conducive to the adsorption and loading of EFD and magnetic substances. The BET specific surface area of EFD&C was $640.49 \text{ m}^2/\text{g}$, which was lower than that of biochar. This was caused by the carbon-based materials loaded from electric furnace dust. The average pore diameter measured by EFD&C was 2.24 nm and the pore volume was $0.36 \text{ cm}^3/\text{g}$, which prepared the conditions for the loading of CH_3ONa . After impregnating with CH_3ONa solution, the adsorption isotherm of SM@EFD&C catalyst was type III, the BET specific surface area and pore volume decreased to $8.01 \text{ m}^2/\text{g}$ and $0.03 \text{ cm}^3/\text{g}$, respectively. It can be attributed to the partial collapse of the carbon-based surface and the pore structure of Na_2CO_3 attached to the carbon-based surface. The average pore diameter of the SM@EFD&C catalyst increased from 2.24 nm to 16.81 nm of the partial collapse of the carbon-based surface caused the reduction of small pores and the formation of mesopores. After Na_2CO_3 was attached to the pore structure of the carbon-based surface, the relative number of mesopores and macropores increased, resulting in an increase in the average pore diameter.

3.6 Vibrating Sample Magnetometer

In Fig. 6, in order to understand the magnetic properties of reed biochar, EFD&C and SM@EFD&C catalysts, they were characterized by vibrating sample magnetometer (VSM). The hysteresis loops of EFD&C and SM@EFD&C catalysts were symmetrical “S” curves without hysteresis, they had super magnetic compliance. The saturation magnetization of reed biochar and EFD&C were 0.06 and $10.69 \text{ Am}^2/\text{kg}$, it can be seen that magnetic materials such as $\text{Fe}_{11}\text{Co}_5$ and MgFe_2O_4 were produced, and the cobalt-iron alloy had high saturation magnetization [52]. The magnetization intensity of SM@EFD&C catalyst was $12.10 \text{ Am}^2/\text{kg}$, compared with EFD&C, the magnetization intensity of SM@EFD&C catalyst

was strengthened, which can be attributed to the formation of Fe_3C magnetic substance [53]. The illustration showed the magnetic properties of the SM@EFD&C catalyst in Fig. 6. The dispersed catalyst can be separated from the reaction product by an external magnetic field within 1 min.

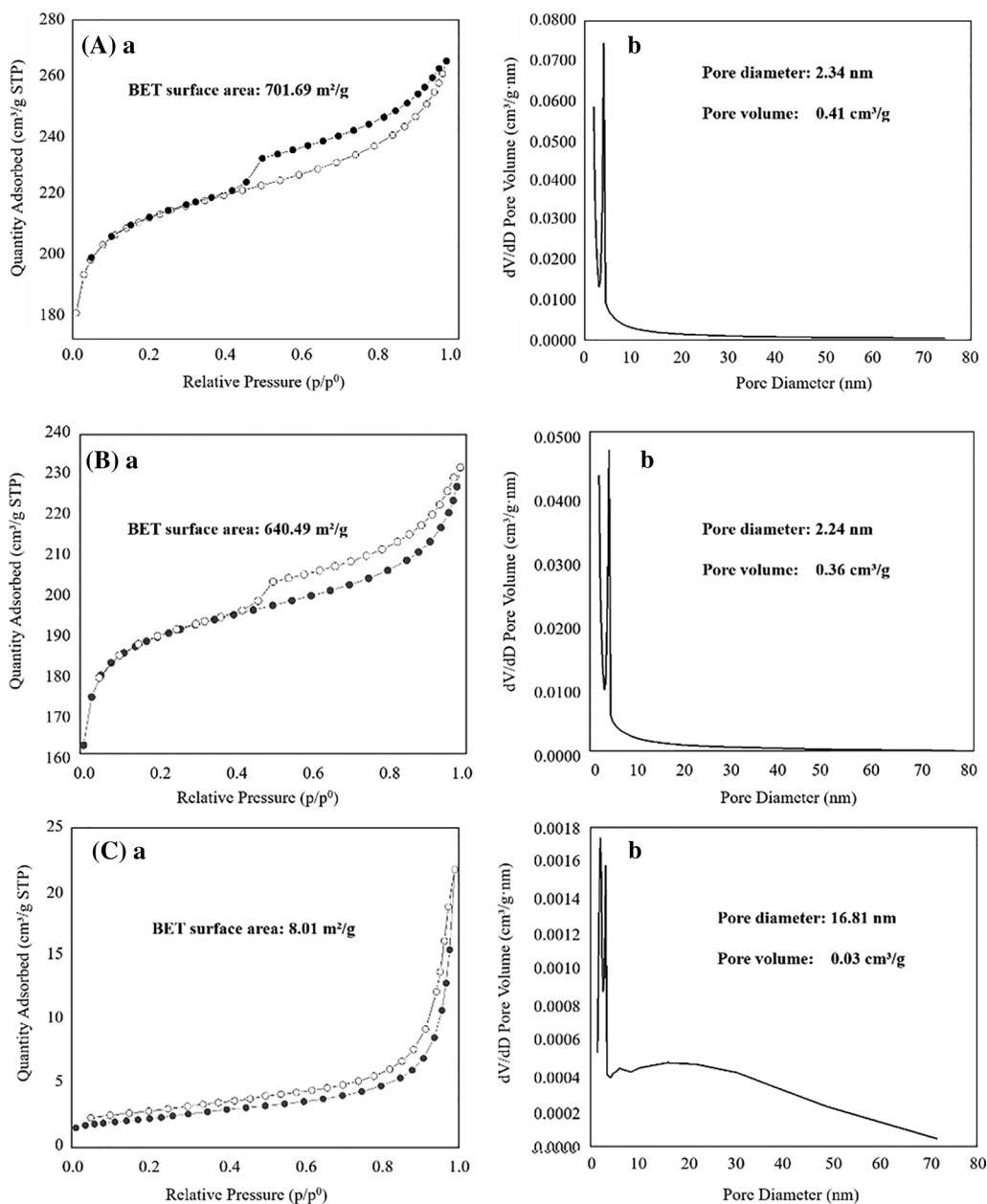


Figure 5: BET analysis for (a) Adsorption-desorption isotherm, and (b) Pore volume and pore diameter of (A) reed biochar, (B) EFD&C, (C) SM@EFD&C

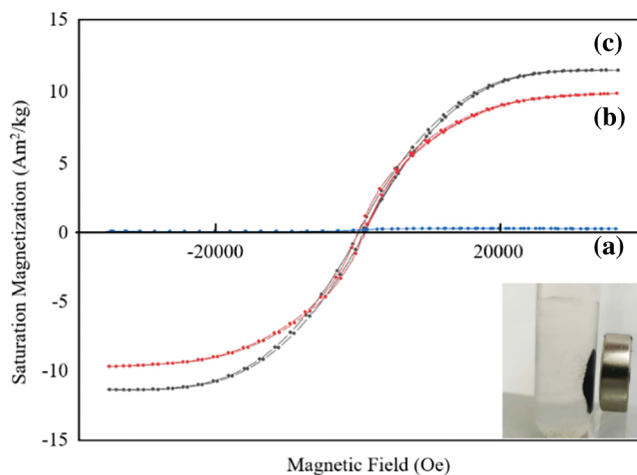


Figure 6: Hysteresis loops of (a) Reed biochar, (b) EFD&C and (c) SM@EFD&C

3.7 Temperature Programmed Desorption of CO₂

The CO₂-TPD curves of the reed biochar, EFD&C and SM@EFD&C catalysts were shown in Fig. 7. The basicity of reed biochar was 0.57 mmol/g, while the alkalinity of EFD&C decreased to 0.42 mmol/g. As we all know, ash was alkaline [54], and the pretreatment of the reed with hydrochloric acid solution reduced the ash content [55], which leads to a decrease in alkalinity. After impregnation with CH₃ONa, the basicity of SM@EFD&C was 0.58 mmol/g, which was due to the increase of basicity caused by the formation of Na₂CO₃ on the carbon-based surface.

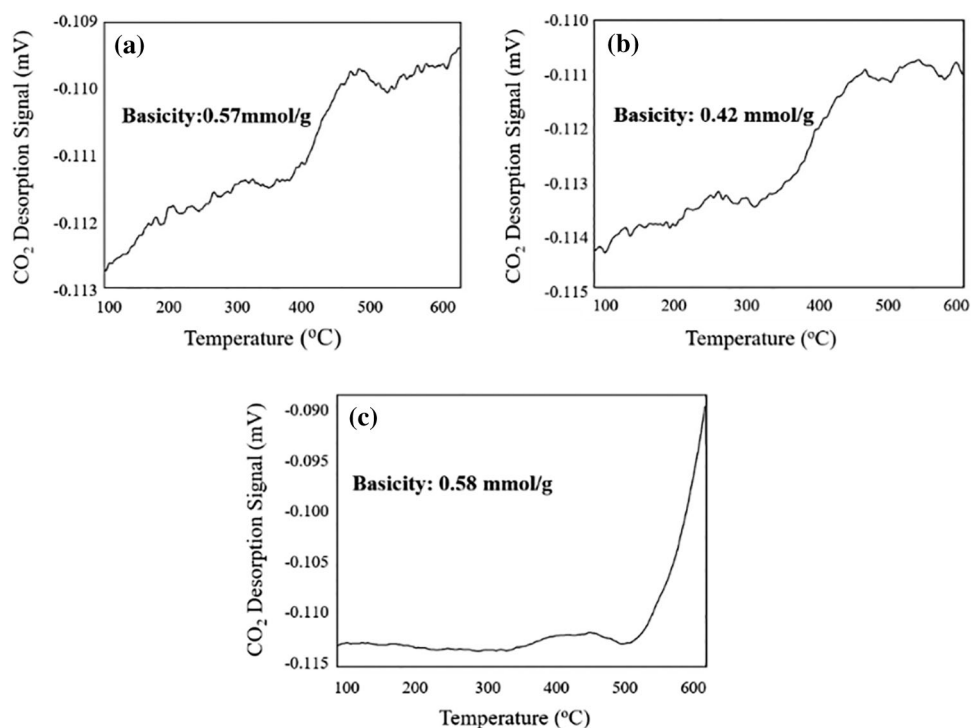


Figure 7: CO₂-TPD analysis (a) Reed biochar, (b) EFD&C and (c) SM@EFD&C

3.8 TG-DTG Analysis

Thermogravimetric analysis was performed to analyze the catalyst thermal behavior by measuring the mass variation in the sample during heating. The TG and DTG curves of reed biochar EFD&C and SM@EFD&C were shown in Fig. 8. In the temperature range of 30–100°C, a significant mass loss was observed in three samples, which can be attributed to the evaporation and removal of water molecules and impurities physically adsorbed in the three materials [56]. The SM@EFD&C lost more mass at this stage, because Na_2CO_3 had strong water absorption, so it will absorb more water from the air than the other two samples. The second mass loss of SM@EFD&C catalyst occurred in the range of 800–900°C, probably due to the loss of CO_2 from the reaction of Na_2CO_3 with oxides. Therefore, the high temperature activation temperature of the catalyst should be lower than 800°C. We calculated that the mass loss of reed straw into biochar was about 70.24% after being calcined at 600°C, indicating that the lignin and cellulose in the reed straw were relatively completely decomposed. In combination with Figs. 8(A) and 8(B), it can be seen that the carbon content was relatively high and the carrier structure was relatively stable under this condition. After the second calcination, the catalyst was reduced from 1.34 g to 0.82 g, and the mass loss was about 38.81%. These losses included evaporation of water and the emission of gas generated by the reaction of carbon and sodium carbonate in the catalyst.

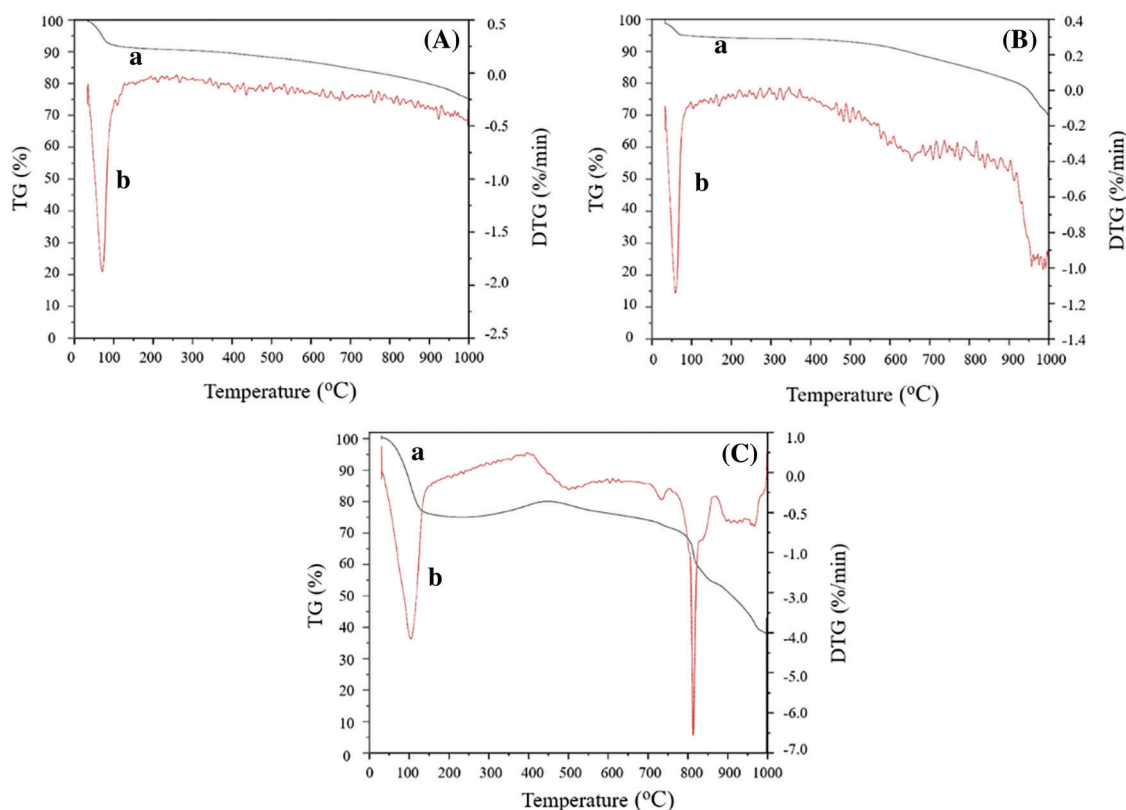
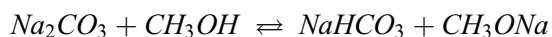
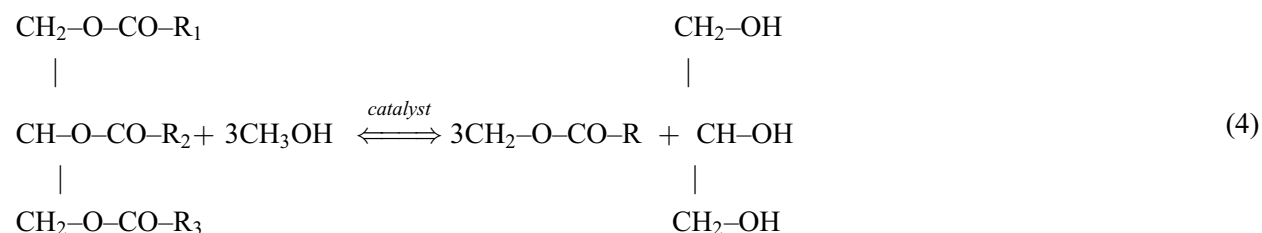


Figure 8: TG–DTG cures (a) TG and (b) DTG of (A) reed biochar, (B) EFD&C and (C) SM@EFD&C

3.9 Application Performance Test

Firstly, the catalytic performance of reed biochar, EFD&C and SM@EFD&C were tested. The results showed that reed biochar and EFD&C were almost inactive at 65°C for 2 h, and the yield of biodiesel was only 4.88 wt% and 0.03 wt%. However, when the SM@EFD&C catalyst was used with biodiesel

yield of 93.14 wt%, indicating that SM@EFD&C had good catalytic activity. Through the above characterization analysis and performance test, it can be known that the catalytic activity of SM@EFD&C catalyst came from sodium methoxide. CH_3ONa was converted into Na_2CO_3 by impregnation and high-temperature calcination, which formed the alkaline active site supported by EFD&C. Fe_3C , $\text{Fe}_{11}\text{Co}_5$ and MgFe_2O_4 provided magnetic sources for the catalyst and were not active substances. Therefore, SM@EFD&C catalyst can be classified as a solid alkali magnetic catalyst, and the overall reaction equation for biodiesel preparation was shown in Formula (4) [57]. The main catalytic mechanism was as follows [58]: Firstly, methanol and triglyceride were adsorbed to the surface of the catalyst, which can be accelerated by magnetic agitation. H^+ was extracted from methanol through the alkaline site of the catalyst to form methanol anion (CH_3O^-) as shown in Formula (5) [59]:



The CH_3O^- produced was a real transesterification reaction catalyst. The carbon atoms in the carbonyl group of triglycerides were attacked by CH_3O^- to form a tetrahedral intermediate. A tetrahedral intermediate was formed by CH_3O^- attack on a carbonyl carbon in the triglycerides. The tetrahedral intermediate broke down into a fatty acid ester and a diglyceride anion. It was then transferred to the diester ion of glycerol for proton regeneration catalytic activity. This sequence was then repeated twice to yield first a monoglyceride intermediate and finally the glycerol product and biodiesel. Compared with acid catalysts, base catalysts seem to take a more direct route to activate the CH_3O^- catalytic active substance reaction, resulting in faster catalytic activity. The SM@EFD&C catalyst was cyclically tested to objectively evaluate its stability.

In the process of testing the stability of the catalyst, the reaction products and the catalyst were separated by external magnetic force, the cyclic test was carried out according to the original catalytic conditions without any treatment of the catalyst. After seven cycles of testing, the yield of biodiesel still reached 89.84 wt%, and decreased to 43.66 wt% in the eighth cycle. It was showed the reusability of the catalyst in the transesterification of soybean oil with methanol in Fig. 9. The decrease of catalytic activity after the fourth recycling was may be caused by two main reasons: (i) one of the reasons may be due to the loss of catalyst in the recovery process [60]. (ii) the other reason may be a dissolution of active substance in the catalyst. Na_2CO_3 was slightly dissolved in glycerol/methanol solution [59]. Therefore, as the number of cycles increased, more and more Na_2CO_3 was dissolved in glycerol/methanol solution or lost in the recovery process, resulting in a decrease in activity. In a nutshell, it showed that SM@EFD&C catalyst had good stability. Therefore, it can be proved that SM@EFD&C catalyst was feasible in terms of activity and stability.

In addition, the catalytic activity and stability of SM@EFD&C catalyst were compared with the commonly employed reported solid base carbon catalysts. The results were shown in Table 2. With regard to the yields of biodiesel, it was noticed that the yields obtained are comparable, lower or higher in some cases than those obtained by other catalysts previously reported in the literature. However, in terms of stability, SM@EFD&C catalyst had good recyclable performance. Of course, whether the catalytic activity or stability, which may be related to the type of oil, reaction conditions, the amount of catalyst and other factors.

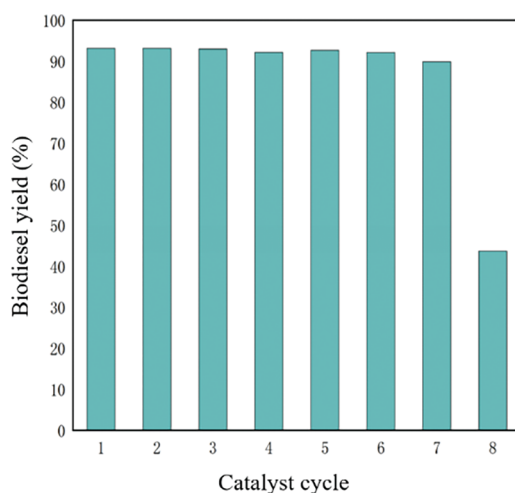


Figure 9: Catalyst cycle of SM@EFD&C

Table 2: Comparison of the efficiency of SM@EFD&C catalyst with some reported catalysts

Carbon based catalysis type	Reaction conditions	Biodiesel yield	Stability	Reference
Kraft lignin carbon loading K_2CO_3 as solid catalyst	65°C for 2 h	99.6%	82.1% for 4 times	[59]
Carbon-supported Na, Ca-based catalysts	60°C for 3 h	91%	75% for 4 times	[43]
Carbon-based MgO catalysts	75°C for 1 h	96.5%	80.2% for 5 times	[61]
High mesoporous activated carbon catalyst prepared from Palm shell carbon based K_2CO_3 and CuO	70°C for 2 h	95.36%	82.5% for 5 times	[62]
A solid base catalyst developed based on activated carbon loaded KOH derived from waste tires	60°C for 2 h	94.50%	80% for 4 times	[63]
Reed magnetic biochar was used as carrier and loaded with CH_3ONa	65°C for 2 h	93.14%	89.8% for 7 times	This work

4 Conclusion

The SM@EFD&C magnetic catalyst was synthesized by impregnation and high-temperature calcination using two solid wastes of reed straw and EFD powder as raw materials. Characterization and analysis showed that SM@EFD&C catalyst had a porous structure and good magnetic properties, and its magnetic sources were $Fe_{11}Co_5$, $MgFe_2O_4$ and Fe_3C . Without optimizing the SM@EFD&C catalyst, biodiesel yield was 93.14 wt%, after seven cycles the yield still reached 89.84 wt%, showing excellent catalytic activity and stability. This research not only provided a certain reference value for the preparation of low-cost and high-efficiency magnetic carbon-based catalysts, but also provided a feasible solution for the reuse of solid waste and the preparation of new materials.

Acknowledgement: The authors wish to acknowledge the financial support from National Natural Science Foundation of China (Nos: 52004095, 51704119, and 21878161), the Natural Science Foundation of Hebei Province (E2017209243) and Department of Education of Hebei Province (BJ2019038).

Funding Statement: The authors received no specific funding for this study.

Conflicts of Interest: The authors declare that they have no conflicts of interest to report regarding the present study.

References

1. The Lancet Planetary Health (2018). Can the Paris agreement save us from a climate catastrophe? *The Lancet Planetary Health*, 2(4), e140. DOI 10.1016/S25425196(18)30056-1.
2. Akdag, S., Yldrm, H. (2020). Toward a sustainable mitigation approach of energy efficiency to greenhouse gas emissions in the European countries. *Heliyon*, 6(3), e03396. DOI 10.1016/j.heliyon.2020.e03396.
3. Uddin, M. N., Taweekun, J., Techato, K., Rahman, M. A., Mofijur, M. et al. (2019). Sustainable biomass as an alternative energy source: Bangladesh perspective. *Energy Procedia*, 160, 648–654. DOI 10.1016/j.egypro.2019.02.217.
4. Field, C. B., Campbell, J. E., Lobell, D. B. (2008). Biomass energy: The scale of the potential resource. *Trends in Ecology & Evolution*, 23(2), 65–72. DOI 10.1016/j.tree.2007.12.001.
5. Guo, H. (2017). Application review of biomass energy and its application prospect in rural areas in China. *Journal of Chinese Agricultural Mechanization*, 38(3), 77–81. DOI 10.13733/j.jcam.issn.20955553.2017.03.018.
6. Mandal, A., Singh, N., Purakayastha, T. J. (2017). Characterization of pesticide sorption behaviour of slow pyrolysis biochars as low cost adsorbent for atrazine and imidacloprid removal. *Science of the Total Environment*, 577, 376–385. DOI 10.1016/j.scitotenv.2016.10.204.
7. Zhang, J. O., Li, C. B., Li, G. T., He, Y., Zhang, J. X. et al. (2021). Effects of biochar on heavy metal bioavailability and uptake by tobacco (*Nicotiana tabacum*) in two soils. *Agriculture Ecosystems & Environment*, 317, 107453. DOI 10.1016/j.agee.2021.107453.
8. Teixidó, M., Hurtado, C., Pignatello, J. J., Beltrán, J. L., Granados, M. et al. (2013). Predicting contaminant adsorption in black carbon (biochar)-amended soil for the veterinary antimicrobial sulfamethazine. *Environmental Science & Technology: ES&T*, 47(12), 6197–6205. DOI 10.1021/es400911c.
9. Oladele, S. O., Adetunji, A. T. (2021). Agro-residue biochar and N fertilizer addition mitigates CO₂-C emission and stabilized soil organic carbon pools in a rain-fed agricultural cropland. *International Soil and Water Conservation Research*, 9(1), 76–86. DOI 10.1016/j.iswcr.2020.09.002.
10. Qin, F. Z., Peng, Y. J., Song, G., Fang, Q. X., Wang, R. Z. et al. (2020). Degradation of sulfamethazine by biochar-supported bimetallic oxide/persulfate system in natural water: Performance and reaction mechanism. *Journal of Hazardous Materials*, 398, 122816. DOI 10.1016/j.jhazmat.2020.122816.
11. Magnus, S., Henrik, L., Verania, A., Gerard, C. (2014). Environmental and socioeconomic impacts of utilizing waste for biochar in rural areas in Indonesia—a systems perspective. *Environmental Science & Technology*, 48(9), 4664–4671. DOI 10.1021/es405190q.
12. Wei, D., Li, B., Huang, H., Luo, L., Zhang, J. et al. (2018). Biochar-based functional materials in the purification of agricultural wastewater: Fabrication, application and future research needs. *Chemosphere*, 197, 165–180. DOI 10.1016/j.chemosphere.2017.12.193.
13. Lehmann, J. (2007). A handful of carbon. *Nature*, 447, 143–144. DOI 10.1038/447143a.
14. Dolrudee, J., Parncheewa, U., Nuwong, C., Apiluck, E. U. (2019). Preparation of carbon supported catalyst from cattail leaves for biodiesel fuel upgrading application. *Materials Today: Proceedings*, 17(Pt4), 1319–1325. DOI 10.1016/j.matpr.2019.06.149.
15. Qiu, Z. Z., Zhai, Y. B., Li, S. H., Liu, X. M., Liu, X. P. et al. (2020). Catalytic co-pyrolysis of sewage sludge and rice husk over biochar catalyst: Bio-oil upgrading and catalytic mechanism. *Waste Management*, 114, 225–233. DOI 10.1016/j.wasman.2020.07.013.

16. Foroutana, R., Mohammadia, R., Razeghib, J., Ramavandicd, B. (2021). Biodiesel production from edible oils using algal biochar/CaO/K₂CO₃ as a heterogeneous and recyclable catalyst. *Renewable Energy*, 168, 1207–1216. DOI 10.1016/j.renene.2020.12.094.
17. Li, H., Dai, T. L., Chen, J. A., Chen, L., Li, Y. X. et al. (2021). Enhanced sludge dewaterability by Fe-rich biochar activating hydrogen peroxide: Co-hydrothermal red mud and reed straw. *Journal of Environmental Management*, 296, 113239. DOI 10.1016/j.jenvman.2021.113239.
18. Wang, X. Z., Deng, Y. H., Luo, J. Y., Chen, M., Xie, S. H. et al. (2010). Study on reed medium density fiberboard. *China Forest Products Industry*, 37(2), 19–21, 25. DOI 10.19531/j.issn1001-5299.2010.02.007.
19. Zhu, Y., Xin, F., Chang, Y., Zhao, Y., Wong, W. C. (2015). Feasibility of reed for biobutanol production hydrolyzed by crude cellulase. *Biomass & Bioenergy*, 76, 24–30. DOI 10.1016/j.biombioe.2015.02.013.
20. Stefanova, A., Aromaa, J., Forsen, O. (2015). Alkaline leaching of zinc from stainless steel electric arc furnace dusts. *Physicochemical Problems of Mineral Processing*, 51(1), 293–302. DOI 10.1016/j.mineng.2005.08.013.
21. Omran, M., Fabritius, T., Guo, C., He, A. (2019). Microwave absorption properties of steelmaking dusts: Effects of temperature on the dielectric constant (ϵ') and loss factor (ϵ'') at 1064 MHz and 2423 MHz. *RSC Advances*, 9(12), 6859–6870. DOI 10.1039/C9RA00009G.
22. Kamali, M., Sheibani, S., Ataie, A. (2021). Magnetic MgFe₂O₄-CaFe₂O₄ s-scheme photocatalyst prepared from recycling of electric arc furnace dust. *Journal of Environmental Management*, 290, 112609. DOI 10.1016/j.jenvman.2021.112609.
23. Hitam, C. N. C., Jalil, A. A. (2020). A review on exploration of Fe₂O₃ photocatalyst towards degradation of dyes and organic contaminants. *Journal of Environmental Management*, 258, 110050. DOI 10.1016/j.jenvman.2019.110050.
24. Rawat, I., Kumar, R. R., Mutanda, T., Bux, F. (2011). Dual role of microalgae: Phycoremediation of domestic wastewater and biomass production for sustainable biofuels production. *Applied Energy*, 88(10), 3411–3424. DOI 10.1016/j.apenergy.2010.11.025.
25. Zabeti, M., Wan, M., Aroua, M. K. (2009). Activity of solid catalysts for biodiesel production: A review. *Fuel Processing Technology*, 90(6), 770–777. DOI 10.1016/j.fuproc.2009.03.010.
26. Talebian-Kiakalaieh, A., Amin, N. A. S., Mazaheri, H. (2013). A review on novel processes of biodiesel production from waste cooking oil. *Applied Energy*, 104, 683–710. DOI 10.1016/j.apenergy.2012.11.061.
27. Saka, C. (2012). BET, TG–DTG, FT-IR, SEM, iodine number analysis and preparation of activated carbon from acorn shell by chemical activation with ZnCl₂. *Journal of Analytical & Applied Pyrolysis*, 95, 21–24. DOI 10.1016/j.jaap.2011.12.020.
28. Wang, Y. T., Fang, Z., Yang, X. X. (2017). Biodiesel production from high acid value oils with a highly active and stable bifunctional magnetic acid. *Applied Energy*, 204, 702–714. DOI 10.1016/j.apenergy.2017.07.060.
29. Wen, Y., He, K., Zhu, Y. J., Han, F. D., Xu, Y. H. et al. (2014). Expanded graphite as superior anode for sodium-ion batteries. *Nature Communications*, 5, 4033, DOI 10.1038/ncomms5033.
30. Chu, H. R., Chen, P., Yu, Q., Xu, D. W. (2018). Preparation and microwave absorption properties of FeCo/Graphene. *Chinese Journal of Materials Research*, 32(3), 161–167. DOI 10.11901/1005.3093.2017.339.
31. Gao, C. B., Xu, P. F., Ruan, F., Li, H. X. (2021). Study on preparation of Fe/Fe₂SiO₄-based cermets by microwave in-situ reduction. *Iron Steel Vanadium Titanium*, 42(3), 135–142. DOI 10.7513/j.issn.1004-7638.2021.03.021.
32. Shen, N. (2006). *Thermal analysis of magnesium ferrite synthetic process (Master Thesis)*. University of Science and Technology Liaoning. China.
33. Cazetta, A. L., Pezoti, O., Bedin, K. C., Silva, T. L., Almeida, V. C. (2016). Magnetic activated carbon derived from biomass waste by concurrent synthesis: Efficient adsorbent for toxic dyes. *ACS Sustainable Chemistry*, 4(3), 1058–1068. DOI 10.1021/acssuschemeng.5b01141.
34. Lillo-Ródenas, M. A., Cazorla-Amorós, D., Linares-Solano, A. (2003). Understanding chemical reactions between carbons and NaOH and KOH: An insight into the chemical activation mechanism. *Carbon*, 41(2), 267–275. DOI 10.1016/S0008-6223(02)00279-8.

35. Freitas, J. C. C., Schettino, M. A., Cunha, A. G., Emmerich, F. G., Bloise, A. C. et al. (2006). NMR investigation on the occurrence of Na species in porous carbons prepared by NaOH activation. *Carbon*, 45(5), 1097–1104. DOI 10.1016/j.carbon.2006.12.006.
36. Siddiqui, M., Nizamuddin, S., Mubarak, N. M., Shirin, K., Aijaz, M. et al. (2017). Characterization and process optimization of biochar produced using novel biomass, waste pomegranate peel: A response surface methodology approach. *Waste & Biomass Valorization*, 10, 521–532. DOI 10.1007/s12649-017-0091-y.
37. Thaveemas, P., Chuenchom, L., Kaowphong, S., Techasakul, S., Saparpakorn, P. et al. (2021). Magnetic carbon nanofiber composite adsorbent through green *in-situ* conversion of bacterial cellulose for highly efficient removal of bisphenol A. *Bioresource Technology*, 333, 125184. DOI 10.1016/j.biortech.2021.125184.
38. Fu, X. B., Li, D. H., Chen, J., Zhang, Y. M., Huang, W. Y. et al. (2013). A microalgae residue based carbon solid acid catalyst for biodiesel production. *Bioresource Technology*, 146, 767–770. DOI 10.1016/j.biortech.2013.07.117.
39. Niu, Y. L., Huang, X. Q., Hu, W. H. (2016). Fe₃C nanoparticle decorated Fe/N doped graphene for efficient oxygen reduction reaction electrocatalysis. *Journal of Power Sources*, 332, 305–311. DOI 10.1016/j.jpowsour.2016.09.130.
40. Pradeep, A., Priyadharsini, P., Chandrasekaran, G. (2008). Sol–gel route of synthesis of nanoparticles of MgFe₂O₄ and XRD, FT-IR and VSM study. *Journal of Magnetism and Magnetic Materials*, 320(21), 2774–2779. DOI 10.1016/j.jmmm.2008.06.012.
41. Joshi, S., Kalyanasundaram, S., Balasubramanian, V. (2013). Quantitative analysis of sodium carbonate and sodium bicarbonate in solid mixtures using fourier transform infrared spectroscopy (FT-IR). *Applied Spectroscopy. Society for Applied Spectroscopy*, 67(8), 841–845. DOI 10.1366/12-06915.
42. Huang, J. Q., Zhang, B., Xu, Z. L., Abouali, S., Kim, J. K. (2015). Novel interlayer made from Fe₃C/carbon nanofiber webs for high performance lithium–sulfur batteries. *Journal of Power Sources*, 285, 43–50. DOI 10.1016/j.jpowsour.2015.02.140.
43. Faria, D. N., Cipriano, D. F., Schettino, M. A., Neto, A. C., Cunha, A. G. et al. (2020). Na, Ca-based catalysts supported on activated carbon for synthesis of biodiesel from soybean oil. *Materials Chemistry and Physics*, 249, 123173. DOI 10.1016/j.matchemphys.2020.123173.
44. Zhang, S., Zhu, N. W., Mao, F. L., Zhang, J., Huang, X. X. et al. (2020). A novel strategy for harmlessness and reduction of copper smelting slags by alkali disaggregation of fayalite (Fe₂SiO₄) coupling with acid leaching. *Journal of Hazardous Materials*, 402, 123791. DOI 10.1016/j.jhazmat.2020.123791.
45. Alomairy, S., Al-Buriahi, M. S., Wahab, E. A. A., Sriwunkum, C., Shaaban, K. S. (2021). Synthesis, FT-IR, and neutron/charged particle transmission properties of Pb₃O₄-SiO₂-ZnO-WO₃ glass system. *Ceramics International*, 47(12), 17322–17330. DOI 10.1016/j.ceramint.2021.03.045.
46. Jafar, M., Monire, R. (2017). Studies on optimization of efficient parameters for removal of lead from aqueous solutions by natural zeolite as a low-cost adsorbent using response surface methodology. *Advances in Environmental Technology*, 3(2), 99–108. DOI 10.22104/aet.2017.1928.1092.
47. Sun, Y. Q., Zhang, Z. T., Liu, L. L., Wang, X. D. (2015). FT-IR, Raman and nmr investigation of CaO-SiO₂-P₂O₅ and CaO-SiO₂-TiO₂-P₂O₅ glasses. *Journal of Non-Crystalline Solids*, 420, 26–33. DOI 10.1016/j.jnoncrysol.2015.04.017.
48. Siddiqui, M. T. H., Nizamuddin, S., Mubarak, N. M., Shirin, M., Aijaz, M. et al. (2019). Characterization and process optimization of biochar produced using novel biomass, waste pomegranate peel: A response surface methodology approach. *Springer Netherlands*, 10(3), 521–532. DOI 10.1007/s12649-017-0091-y.
49. Liu, X. Q., Ding, H. S., Wang, Y. Y., Liu, W. J., Jiang, H. (2016). Pyrolytic temperature dependent and ash catalyzed formation of sludge char with ultra-high adsorption to 1-naphthol. *Environmental Science & Technology*, 50(5), 2602–2609. DOI 10.1021/acs.est.5b04536.
50. Liu, S., Ge, X. M., Liu, Z., Li, Y. B. (2016). Effect of harvest date on *Arundo donax* L. (giant reed) composition, ensilage performance, and enzymatic digestibility. *Bioresource Technology*, 205, 97–103. DOI 10.1016/j.biortech.2016.01.011.

51. Chang, Y. H., Lin, C. L., Hsu, Y. H., Lin, J. H. (2021). Medium effect on acid degradation of cotton and wood celluloses. *Industrial Crops & Products*, 167, 113540. DOI 10.1016/j.indcrop.2021.113540.
52. Kozyatnyk, I., Oesterle, P., Wurzer, C., Mašek, O., Jansson, S. (2021). Removal of contaminants of emerging concern from multicomponent systems using carbon dioxide activated biochar from lignocellulosic feedstocks. *Bioresource Technology*, 340, 125561. DOI 10.1016/j.biortech.2021.125561.
53. Sotirios, K., Rasmus, B. K., Michael, E., Rasmus, F. (2017). Synthesis and characterization of iron-cobalt (FeCo) alloy nanoparticles supported on carbon. *Journal of Alloys and Compounds*, 725, 1210–1216. DOI 10.1016/j.jallcom.2017.07.105.
54. Soriano, L., Font, A., Tashima, M. M., Monzó, J., Borrachero, M. V. et al. (2021). Almond-shell biomass ash (ABA): A greener alternative to the use of commercial alkaline reagents in alkali-activated cement. *Construction and Building Materials*, 290, 123251. DOI 10.1016/j.conbuildmat.2021.123251.
55. Xiao, Y., Raheem, A., Ding, L., Chen, W. H., Chen, X. L. et al. (2022). Pretreatment, modification and applications of sewage sludge-derived biochar for resource recovery-A review. *Chemosphere*, 287, 131969. DOI 10.1016/j.chemosphere.2021.131969.
56. Lourenço, M. E. K., Arrais, G. M., Souza, D. L. P. T., Narciso, D. R. F. G., Roberto, Z. J. et al. (2021). Acai seed ash as a novel basic heterogeneous catalyst for biodiesel synthesis: Optimization of the biodiesel production process. *Fuel*, 299, 120887. DOI 10.1016/j.fuel.2021.120887.
57. Leung, D. Y. C., Wu, X., Leung, M. K. H. (2009). A review on biodiesel production using catalyzed transesterification. *Applied Energy*, 87(4), 1083–1095. DOI 10.1016/j.apenergy.2009.10.006.
58. Helwani, Z., Othman, M. R., Aziz, N., Kim, J., Fernando, W. J. N. (2009). Solid heterogeneous catalysts for transesterification of triglycerides with methanol: A review. *Applied Catalysis A: General*, 363(1), 1–10. DOI 10.1016/j.apcata.2009.05.021.
59. Malins, K. (2018). The potential of K_3PO_4 , K_2CO_3 , Na_3PO_4 and Na_2CO_3 as reusable alkaline catalysts for practical application in biodiesel production. *Fuel Processing Technology*, 179, 302–312. DOI 10.1016/j.fuproc.2018.07.017.
60. Li, X. F., Zuo, Y., Zhang, Y., Fu, Y., Guo, Q. X. (2013). In situ preparation of K_2CO_3 supported Kraft lignin activated carbon as solid base catalyst for biodiesel production. *Fuel*, 113, 435–442. DOI 10.1016/j.fuel.2013.06.008.
61. Du, L. X., Li, Z., Ding, S. X., Chen, C., Qu, S. K. et al. (2019). Synthesis and characterization of carbon-based MgO catalysts for biodiesel production from castor oil. *Fuel*, 258, 116122. DOI 10.1016/j.fuel.2019.116122.
62. Fadzilah, A. R., Umer, R., Lokman, I. M., Balkis, H., Fahad, A. et al. (2021). Bifunctional nano-catalyst produced from palm kernel shell via hydrothermal-assisted carbonization for biodiesel production from waste cooking oil. *Renewable and Sustainable Energy Reviews*, 137, 110638. DOI 10.1016/j.rser.2020.110638.
63. Ayoob, A. K., Abdelrahman, B. F. (2020). Valorization of waste tires in the synthesis of an effective carbon based catalyst for biodiesel production from a mixture of non-edible oils. *Fuel*, 264(C), 116754. DOI 10.1016/j.fuel.2019.116754.